Exploring Room Temperature Transport of Single-Molecule Magnets (SMM) based Molecular Spintronics Devices by Using the Magnetic Tunnel Junction (MTJ) as a Device Platform

Pawan Tyagi^{1*}, Christopher Riso¹, Amir Uzma¹, Carlos Rojas-Dotti,² Jose Martínez-Lillo^{2*}

University of the District of Columbia, Department of Mechanical Engineering, 4200 Connecticut Avenue NW Washington DC-20008, USA¹; Instituto de Ciencia Molecular (ICMol), Universitat de València, c/Catedrático José Beltrán, 46980 Paterna, València, Spain²

Corresponding Author Email*: ptyagi@udc.edu and f.jose.martinez@uv.es

Abstract: A device architecture utilizing a single-molecule magnet (SMM) as a device element between two ferromagnetic electrodes may open vast opportunities to create novel molecular spintronics devices. Here we report a method of connecting SMM to the ferromagnetic electrodes. We utilized a nickel (Ni)-AlOx-Ni magnetic tunnel junction (MTJ) with the exposed side edges as a test bed. In the present work, we utilized SMM, with a hexanuclear $[Mn_6(\mu_3-O)_2(H_2N-sao)_6(6-atha)_2(EtOH)_6]$ $[H_2N-saoH = salicylamidoxime, 6-atha = 6-acetylthiohexanoate]$ complex that is attached to alkane tethers terminated with thiols. These Mn based molecules were electrochemically bonded between the two Ni electrodes of an exposed edge tunnel junction that was produced by the lift-off method. SMM treated magnetic tunnel junction exhibited current enhancement and transitory current suppression at room temperature. Monte Carlo simulation was utilized to understand the transport properties of our molecular spintronics device.

Introduction: The single-molecule magnets (SMMs) are one of the most exciting class of molecules possessing tunable spin state for a wide range and exhibited Berry phase like quantum mechanical phenomenon ¹. SMMs are also highly promising for the quantum computation application². However, further advancement in producing SMM-based molecular devices will require an efficient and mass fabrication approach to connect the metallic leads to this type of molecular systems. To date, only planar nanogap junction-based devices, where a planar nanogap separates two gold electrodes, have been utilized ^{2c,3}. Planar nanogap junction approach gives <10% yield and primarily limited to the gold metal serving as source and drain electrode ^{2c}. However, SMMs can behave very differently when connected to a variety of metallic electrodes. One big thrust area in the field of molecular spintronics is the scope of simultaneously connecting an SMM to two ferromagnetic leads placed at the nanoscale gap. It will be intriguing to explore how spin-polarized transport from ferromagnetic electrodes can be used to manipulate and detect spin transport via a SMM with the tunable spin state. The impact of SMM interaction when strongly bonded to two ferromagnetic electrodes, not simply chemisorbed on one ferromagnet, may modify the magnetic properties of the ferromagnetic film itself and hence produce spinterface like devices for novel applications ⁴. The SMM interaction with ferromagnetic electrodes can nucleate local phenomena that may penetrate deep into the ferromagnetic electrodes due to the presence of long-range magnetic ordering within a typical ferromagnet. To advance the possibilities as mentioned above we have attempted to test if magnetic tunnel junctions (MTJ) can be utilized as the testbed to study SMMs. A MTJ is basically a vertical nanogap junction where the gap between two ferromagnetic electrodes can be controlled to angstrom level via controllable thin film deposition in widely available sputtering machines in small and big institutions. To study SMMs we utilized exposed edge MTJ produced by the lift-off methods we established in our previous work⁵. SMMs and insulator make parallel connection between two metal electrodes. This MTJ based molecular spintronic device (MTJMSD) fabrication approach brings enormous advantages over conventional schemes and solves critical issues like oxidation of ferromagnetic electrodes⁶. MTJMSD has been successful in observing a number intriguing and interesting phenomena by enabling magnetic molecule induced strong exchange coupling between ferromagnetic electrodes of a MTJ^{5,7}. Previously, we have utilized this MTJMSD approach to investigate organometallic molecules⁵. Here we report our first experimental results regarding the utilization of MTJMSD approach to investigate transport properties of SMMs at room temperature.

Experimental Details: In this study MTJMSD mainly employed nickel (Ni) as the ferromagnetic electrodes. To identify the temperature, limit up to which Ni could be heated without oxidation, a reflectance vs. temperature study was conducted (Supplementary Material, Fig.S1). MTJ testbed for studying SMM-based molecular devices were fabricated by the liftoff method that has been described in details elsewhere⁸ and also in the supplementary material this for paper (Supplementary Material, Fig. S2). The protocol for this oxidation study is the same as that utilized in our previous work⁶. This reflectance study suggested that Ni film did not show any noticeable change in reflectance up to 90 °C (Fig. S1). Hence, the temperature for MTJMSD's fabrication steps where Ni was in the ambient state was limited to 90 °C. For MTJ testbed fabrication, we utilized Tantalum (Ta) as a seed layer to promote adhesion between the oxidized silicon substrate and bottom Ni electrode. We used alumina (AlOx) as the insulating spacer between the two ferromagnetic electrodes of different thickness. Our MTJ testbed with exposed side edges (Fig. 1a) possessed Ta (5 nm)/Ni (20 nm)/AlOx (2

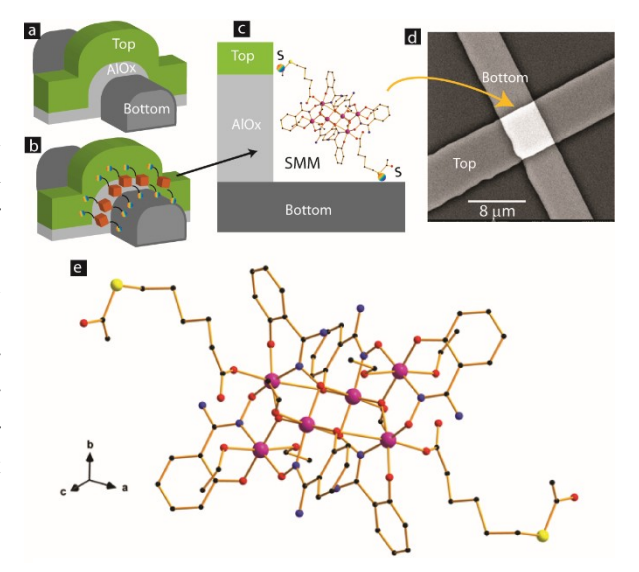


Fig. 1 3D view of MTJ with exposed side edges (a) before and after the bridging of SMMs channels. (c) magnified view of one SMM covalently bonded with two Ni electrodes. (d) SEM of a complete SMM-based MTJMSD. (e) View along the crystallographic [111] direction of the molecular structure of SMM. H atoms and ethanol molecules of crystallization have been omitted for clarity. Color code: pink, Mn; yellow, S; red, O; blue, N; black, C.

nm)/Ni (10 nm) configuration. We kept the different top and bottom electrode thicknesses to produce a difference in magnetic coercivity, to acquire the ability to control the magnetization of thinner film at relatively low magnetic field as compared to thicker Ni film⁹. A 3D perspective view of the exposed side of the MTJ is shown before (Fig. 1a) and after (Fig. 1b) hosting the molecules. Figure 1c shows the connection of each SMM with the two metal electrodes with the help of the thiol functional group. For SMM bridging, all the junctions were simultaneously submerged under the same SMM solution drop. For SMM bridging between Ni electrodes, we utilized the previously published electrochemical method⁸. After molecular treatment, the excess SMM solution was washed off using ethanol. Subsequently, the sample was cleaned and dried before conducting microscopy and transport (I-V) studies.

In the MTJMSD SMMs and insulator make parallel connection between two metal electrodes. Based on SMM size and available exposed lengths, we estimated that ~10,000 SMM could be connected between electrodes. SEM image shows the top view of an MTJMSD (Fig. 1d). The crystal structure of SMM used in this paper has been reported elsewhere¹⁰. Nevertheless, we discuss here certain structural features that are useful to understand SMM characteristics and possible effects on the studied molecular device. The magnified version of the SMM molecular structure is shown in (Fig. 1e). This molecule crystallizes in the monoclinic system with space group $P2_1/c$, and its crystal structure is made up of neutral hexanuclear Mn₆ complexes along with ethanol molecules of crystallization. It has structural features in common with other Mn₆ single-molecule magnets based on the salicylamidoxime ligand¹¹. Each hexanuclear [Mn₆(μ_3 -O)₂(H₂N-sao)₆(6-atha)₂(EtOH)₆] [H₂N-saoH = salicylamidoxime, 6-atha = 6-acetylthiohexanoate] complex contains two symmetry equivalent [Mn₃(μ_3 -O)] triangular moieties, which

are linked by two phenolate and two oximate O-atoms. The six Mn^{III} ions exhibit distorted octahedral geometries with the Jahn-Teller axes approximately perpendicular to the $[Mn_3(\mu_3-O)]$ planes. The monodentate carboxylate ligand is coordinate on Mn(3) and on its symmetry equivalent. The remaining coordination sites on the Mn^{III} ions are occupied by ethanol molecules. The Mn-N-O-Mn torsion angles of the $[Mn_3(\mu_3-O)(H_2N-sao)_3]$ triangular unit are 38.9, 36.5 and 26.0°. The intramolecular $S\cdots S$ separation is ca. 23.0 Å 10 . We studied MTJ testbed, and SMM treated MTJs with SEM and AFM. We utilized Phenom XL SEM and NaioFlex AFM for the microscopy study. The average width of the top and bottom electrodes was in 4-8 μ m range. Generally, MTJ junction's area was ~40 μ m². Current-voltage (I-V) studies were performed on all the MTJs before and after treating with the SMM or bridging SMM channels between two Ni electrodes. For the I-V studies, we utilized Keithley source meters (Model # 2420, Model 6430) connected to biaxial cable and low noise micromanipulator probes placed in a metal Faraday cage.

Results and Discussion: We first focus on ensuring that MTJ testbed are robust and utilized our well established method for producing high quality tunnel barrier^{6-7, 12}. In the MTJMSD approach instabilities in the MTJs are likely to arise due (a) weak tunnel barrier that keep degrading to resistor, (b) high leakage current via spikes at the boarder of photolithographically defined bottom electrode, potential chemical etching of the ferromagnetic electrodes effect of solvent and SMM solution in ethanol. To produce a stable tunnel barrier for this study we utilized the previous optimized AlOx deposition recipe^{12b}. There are several insightful ways to study the anomalies regarding MTJ tunnel barriers¹³. According to empirical understanding a ~2 nm tunnel barrier deposited is mainly impacted by the relaxing mechanical stresses^{12b}. We observed that tunnel barrier that are of high quality generally remain stable or slightly improve over a period of 48 hours (Fig.2a-b). The mechanism behind improvement in tunnel barrier quality is seemingly related to the relaxing mechanical stresses AlOx^{12b};

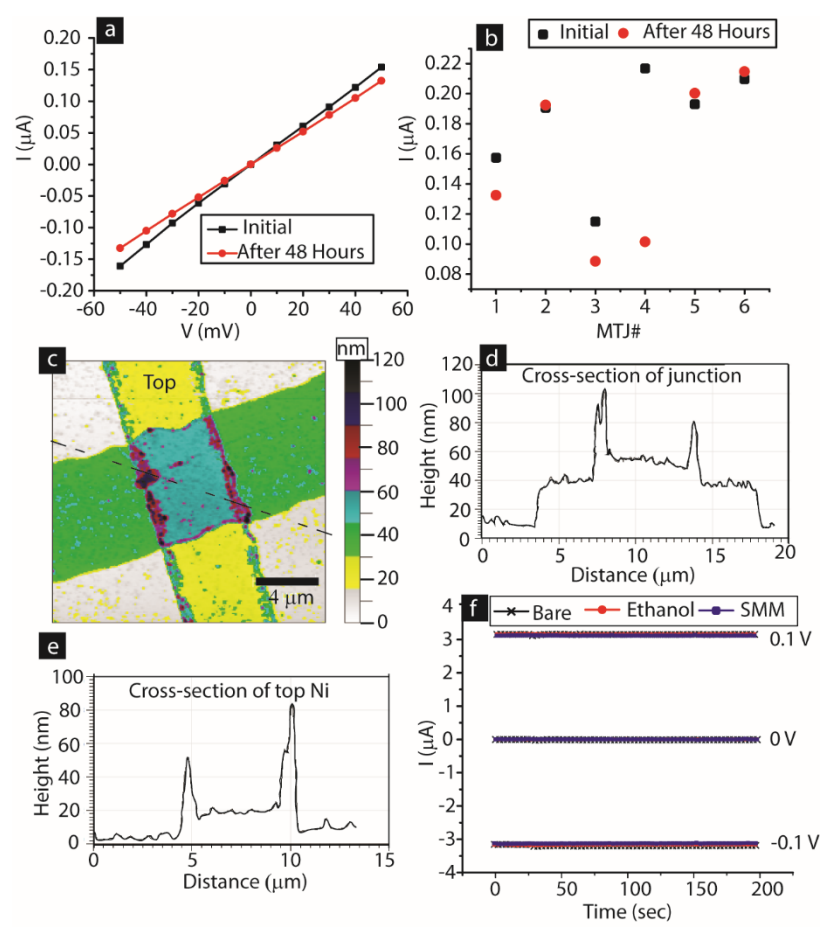


Fig. 2: (a) Representative I-V of a bare MTJ after 48 hours. (b) Variation in current of six MTJs at 50 mV after 48 hours. (c) AFM showing topography of an MTJ. (d) AFM of cross-section of junction along the dashed line in panel (c). (e) AFM of cross section of top Ni electrode. (f) Stability of top Ni electrode state subjected to alternating +/- 0.1 V in bare state, after immersion in ethanol, and after immersion in SMM solution in ethanol solvent.

an in-depth analysis on this topic is beyond the scope this paper. In the present case, MTJ testbeds showed

slight improvement (Fig. 2a). Data is taken from six representative MTJs that did not show any sign of degradation (Fig. 2b).

We also avoided the transport leakage via the notches along the photolithographically defined bottom electrode side edges (Fig.2c-d). According to our previous experience a cross-junction MTJ is highly unstable if side edges of the bottom electrode possess notches. These notches become hot spot of charge transport irrespective of the quality of tunnel barrier in the planar area. Notches at the edge of photolithographically defined thin films were avoided by developing undercut photoresist profile as discussed in our prior work^{12c}. We produced all MTJ testbeds with bottom electrode possessing tapered side edges (Fig. 2c). The AFM cross-sectional image of the junction area shows that bottom electrode was well rounded (Fig. 2d). We did not apply the improvised photolithography recipe of producing tapered edges for the top electrode as top electrode edges do not interfere with the AlOx tunnel barrier stability (Fig. 2e).

We also ensure that MTJ testbed are fully intact after the interaction with SMM solution in ethanol. The AFM study showed in Fig. 2c-d is on an MTJ that was treated with SMM solution in ethanol (SMM dissolved in ethanol). We found that all the nickel electrodes were fully intact and there was no sign of any chemical etching. This AFM study supports the SEM image of an MTJMSD shown in Fig.1d (i.e SEM image of SMM treated MTJ testbed). SEM and AFM study confirm that we did not cause any chemical etching of Ni electrode. To further triple check ethanol solvent or SMM solution in ethanol do not cause damage to electrode that we could notice in the AFM and SEM imaged we conducted transport study via top electrode under different conditions (Fig. 2f). We chose top electrode because this is nearly half

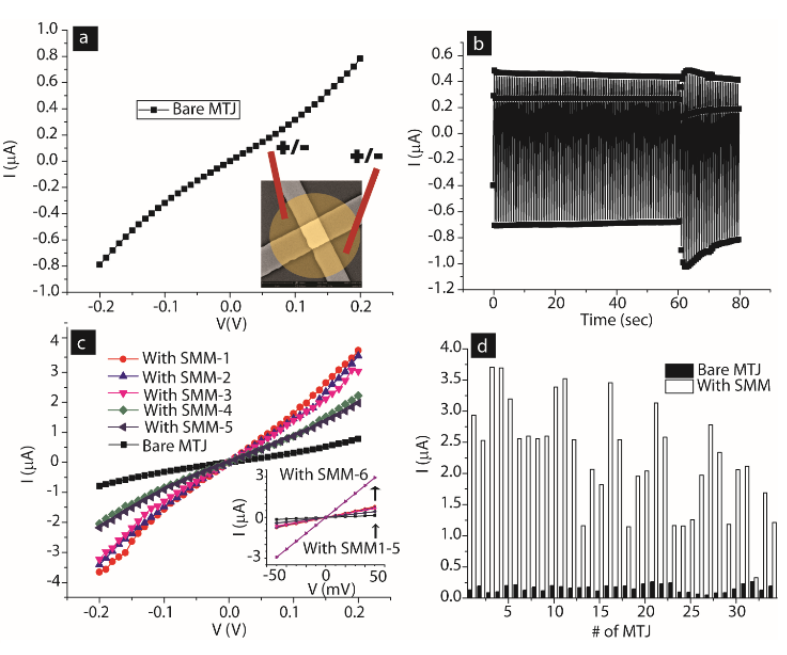


Fig. 3: (a) Representative I-V of a bare MTJ. Inset shows that MTJs were submerged under SMMs solution with two electrodes to apply $\pm 100\,$ mV. (b) Current vs. time spectra recorded between two electrodes placed in molecular solution on an MTJ (c) Multiple I-V showing SMM effect on bare MTJ transport. (d) Histogram of 34 MTJ before and after hosting SMMs channels along the edges.

of the bottom electrode thickness and will be able to respond to chemical etching readily. We alternated bias on bottom electrode between 0.1V and -0.1 V. for 200 sec (Fig. 2f). We could not see any difference in transport via top nickel electrode due to the prolong exposure to ethanol and SMM solution in ethanol. This experiment was repeated three times each for 200 sec and found no change. We also ensured that air exposure do not create any instability by oxidizing the Ni electrodes. We already discussed that our MTJMSD fabrication approach is optimized by utilizing our discovery that the most of the ferromagnets start oxidizing significantly after 90 °C (Fig. S1)⁶. To further verify we also conducted I-V studies after three years of device fabrication and found no change in ~10 nm thick Ni film.

In the prior work, we and other groups have conducted the additional control experiments to prove that molecular channels indeed serve as the effective conductance channel as compared to tunnel barrier⁸,

¹⁴. Multiple prior studies showed the tunnel junction based molecular device ability to reverse the molecule effect on transport^{8, 14-15} and hence unlike other approaches is far more suitable in making reliable molecular devices.

An array of MTJs showing nonlinear I-V (Fig. 3a), a representative characteristic of tunneling type transport, were subjected to the molecular bridging process. The inset image in Fig. 3a only shows the conceptual physical condition for one junction. The actual image of the immersion of all the junctions under the same molecular drop is shown in supplementary material (Supplementary material, Fig.S1). For SMM bridging, all the 34 junctions were simultaneously submerged under the same molecular drop.

Typical current vs. time graph is shown in figure 3b. The I-V of MTJ after interacting with SMM showed a significant increase in MTJ's current (Fig. 3c). This increase in current indicates that SMMs have successfully created additional transport channels across the AlOx tunneling barrier, in agreement with the conceptual picture shown in Fig. 1c and our prior work in the area of MTJMSD^{5, 7a, 8}. The central core of each SMM channels, as per the conceptual drawing Fig.1b-c, are connected to two metal leads via two hexane insulating tethers. The slowest step in transport via SMM channel is expected to be tunneling process via hexane tethers. The length of each hexane tether is < 1 nm, which is much smaller than the ~2 nm AlOx tunneling. Hexane tethers (<1 nm) are also free of structural defects as compared to planar AlOx tunneling barriers (~2 nm). Two hexane tethers of each SMM make a strong Ni-S covalent bond with the Ni metal electrodes resulting in a highly reproducible and well-defined interface (Fig. 1c). Hence, transport via SMM is much more efficient as compared to AlOx and hence leading to a decrease in resistance of MTJ testbed (Fig. 3c). Decrease in overall MTJMSD SMM- and MTJ- based molecular spintronics devices (SMM-MTJMSD) typically settled in the μA level current state. We also observed a similar phenomenon of a reduction in resistance after the bridging of another form of paramagnetic molecules between metal electrodes⁸.

We conducted multiple I-V studies right after SMM treatment to understand any initial dynamic process happening due to SMM and ferromagnetic electrode interactions. Six I-V studies on the freshly formed MTJMSD were different (Fig. 3c). The first three I-V studies were of similar order of magnitude. However, fourth and fifth I-V settled at a transient lower current state (Fig. 3c). Repeating the I-V 6th time set it into the highest current state. This random switching between high, low, and high current state after the SMM bridging is believed to be due to the transient impact of SMM molecules on the ferromagnetic electrodes. SMMs are expected to establish highly efficient spin channels and a strong exchange coupling between the two ferromagnetic electrodes. In the prior study, we observed OMC paramagnetic molecules producing a transient effect that last from several minutes to hours. We are unable to explain the precise dynamics of ferromagnetic electrodes under the impact of molecular exchange coupling in the initial state. Based on our prior work^{5a, 7b}, we believe that SMM like paramagnetic molecules catalyze long range changes on ferromagnets, emanating from the molecule-ferromagnet interfaces. The SMM impacted regions might be propagating deeper into the ferromagnetic electrodes. During this period, a ferromagnetic electrode near junction may experience competition between SMM influenced regions and original ferromagnetic electrode properties (i.e., before SMM interaction). We have previously observed the paramagnetic molecule impact spreading over several micron regions ^{5a, 7b}. Further research may focus on the investigation of the dynamic processes occurring on the freshly produced MTJMSDs.

Impact of SMM was studied on 34 MTJs that were simultaneously treated with SMMs solution to make molecular channels. All the 34 MTJs showed current enhancement (Fig. 4d). This study suggests that our MTJMSD fabrication process can yield nearly 100% device yield, and mainly limited to the number of available MTJ/chip. In our previous work, we also demonstrated that several thousands of MTJ pillars,

without any electrical connections, could be simultaneously transformed into molecular devices 5a . In the present case current for 34 MTJs at 50 mV increased from $0.16\pm0.05~\mu A$ to $2.26\pm0.86~\mu A$ (Fig. 4d).

It is noteworthy that our MTJs consist of Ni ferromagnetic electrodes and SMM paramagnetic molecules. SMM supposedly possesses a net spin state as expected with other SMMs^{1b}. Indeed, this Mn₆ SMM possess spin ground states varying from 4 to 12 at low temperature, depending on their flexible Mn-N-O-Mn torsion angles. In such cases, SMM's spin state has the possibility to interact with the large magnetic ordering of the Ni electrodes via < 1 nm hexane tethers and Ni-S interfaces. It must be noted that hexane molecule is almost perfect tunneling channels with very high spin coherence length and time due to significantly low spin scattering characteristics^{4b}. SMM making covalent bond-based Ni-S interface on the side face of Ni ferromagnets are atomically similar for all the SMMs. SMM-Ni interfaces do not suffer from interfacial roughness encountered in typical MTJ tunnel barriers. Hence, SMM can become a strong bridge between two Ni ferromagnets. In this case, SMM must be viewed as an extended Ni(bulk)-Ni(Molecule affected)-Ni-S-Hexane-[SMM Mn₆ Core]-Hexane-S-Ni-Ni(Molecule affected)-Ni(bulk) system. Our rationale for considering SMM as an extended system is also based on our prior work with another form of MTJMSD involving Octa-metallic Molecular Cluster (OMC) paramagnetic molecules and MTJs. In the previous work, OMC was connected with two NiFe ferromagnetic films using ten carbon long alkane tethers and thiol bonds. In this case, OMCs produced a robust antiferromagnetic coupling between the microscopic ferromagnetic electrodes. OMC induced exchange coupling was stable above 330 K and catalyzed the transformation of magnetic electrodes over several micron areas ^{5a, 7b}. These OMC based MTJMSD provided direct evidence in three independent magnetic measurements that paramagnetic molecules are no longer isolated from electrodes. ^{5b, 7a}. In the context of MTJMSD, an OMC was operating far beyond its physical boundary. MFM like RT experimental studies showed that OMC influence was observed as the extended system of NiFe(bulk)-NiFe(OMC impacted))-Ni-S-Decane-[OMC]-Decane-S-Ni-NiFe(OMC impacted)-NiFe(bulk) system. We also observed several orders of magnitude current suppression on OMC based MTJMSDs that was only possible when ferromagnetic electrodes were impacted away from the physical locations of OMCs ^{5a, 7c}. In the present case, SMM-MTJMSD did not exhibit permanent current suppression. However, SMMs produced transient current suppression on MTJs.

A typical suppressed current state on SMM treated MTJ is shown in Fig. 4a. Repeating I-V studies brought SMM-MTJMSD into the high current state (Fig. 4b). The incubation period, when SMM-MTJMSD was left idle for several hours to days, shifted many SMM-MTJMSD from ~µA level high current state to a suppressed current state (Fig. 4a and c). In some instances, suppressed current states were rather robust and persisted for several hours, as observed during multiple I-V studies (Fig. 4c). Robust suppressed current states were observed from pA level to almost complete current suppression where only noise like feature could be observed (Fig. 4d). The SMM-MTJMSD shown in Fig. 4d resemble with the I-V of MTJ with ~7 nm thick tunnel barrier (Supplementary Material, Fig. S4). Such, noise like features were appeared in multiple studies (Supplementary Material, Fig. S3-S4). The observation of current suppression was observed on 11 SMM treated MTJs (Fig. 4e). Two MTJs, MTJ #1 and MTJ#2 (Fig. 4e) appeared in the suppressed current state right after the bridging of SMMs across the tunneling barrier. In all other cases, SMM-MTJMSD current first increased, and then settled in the temporary suppressed current state, and then again returned to the µA level high current state (Fig. 4e). Two samples, MTJ#2 and MTJ#7, showed current suppression observation twice. We studied MTJMSD for a period of four months. Every time we scanned the 34 junctions, we found 2-6 SMM-MTJMSD in the suppressed current state, but remaining SMM-MTJMSD stayed in the high current state. It was apparent that SMM-MTJMSD stable state is the high current state, as opposed to the stable suppressed current state observed in the prior study^{7a}. We carefully tested electrical leads and connections to ensure that observed current suppression is only coming from SMM-MTJMSD.

According to conventional MTJ based spin valve theory, antiparallel alignment of the magnetizations of the two ferromagnetic films produced the lowest current state ¹⁶. On the other hand, the parallel alignment of the ferromagnetic films produced the highest current state. In the conventional spin-valve devices, an external magnetic field switches the direction of ferromagnetic electrodes between parallel and antiparallel states. According to traditional MTJ spin-valve theory, the difference between the MTJ high and low current state is mainly dependent on the spin polarization properties of the ferromagnetic electrodes. However, the spin polarization property is not the fundamental property of a ferromagnet. Spin polarization heavily depends on the medium present between the two ferromagnetic films. For example, the spin polarization of iron was drastically different when MgO tunnel barrier replaced AlOx tunnel barrier ^{16b, 17}. An SMM like paramagnetic molecule connected to two ferromagnetic electrodes via covalent bonding establishes strong exchange coupling with the two ferromagnetic electrodes impacting the spin density of states^{5a}. If the exchange coupling is significantly strong, one can observe the effect on the

microscopic junction area 7a, 7c. In this paper, the observation of current suppression indicates that SMM produced antiferromagnetic coupling between the two Ni electrodes. If the nature of molecular coupling was ferromagnetic, one could expect the permanent increase in device current. However, presumably unlike our prior work, 7a this SMM induced antiferromagnetic coupling is unable to stabilize current suppression permanently. Also, the SMM core is paramagnetic, and when connected to two ferromagnetic electrodes can influence what type of spin will crossover easily. This phenomenon is called spin filtering and can modify the Ni spin polarization. Our hypothesis that SMM produces spin polarization and antiferromagnetic coupling leading to current suppression is also in agreement with our prior work on a very similar MTJMSD system ^{5a 7a}. To further explain various possibilities of SMM induced exchange coupling between ferromagnetic electrodes, we have discussed Monte Carlo simulations elsewhere in this paper.

We hypothesize that if SMM-MTJMSD's transport is affected by the SMM's induced antiferromagnetic exchange coupling with the magnetic electrodes, then the application of the magnetic field should produce a noticable effect. Next, we investigated the SMM-MTJMSD under magnetic field applied during the electrical measurement. Subjecting SMM-MTJMSD up to ~500 Oe did not yield any noticeable change in magnetic transport (Supplementary Material, Fig. S5). However, magnetizing the SMM-MTJMSD under ~0.2 T magnetic field with the help of a permanent magnet promoted higher current state (Fig. 5a). We noted the five MTJs's current at 50 mV

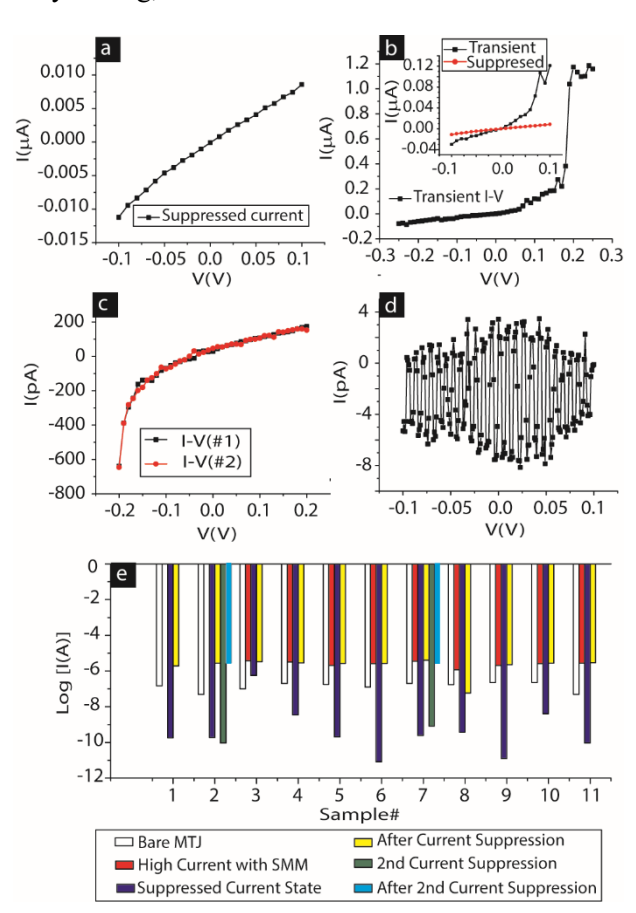


Fig. 4: SMM-MTJMSD showing (a) suppressed current state. (b) nA level suppressed current state transitioning to the high μA level high current state. The suppressed current level could be (c) quite stable or in (d) ultra-low current state where only noise could be recorded. (e) Histogram of 11 MTJ showing suppressed current state after hosting SMM channels between Ni ferromagnetic electrodes.

increased from $0.16\pm0.07~\mu A$ to $1.08\pm0.68~\mu A$ after hosting SMM channels (Fig. 5a). Magnetizing in the

permanent magnetic field further increased the SMM-MTJMSD current to 2.26±0.17 µA (Fig. 5a). We also

attempted to measure the impact of SMM with magnetic measurements. We performed magnetic force microscopy (MFM) by using NaioFlex AFM. To avoid the effect of topography in MFM, we kept 100 nm separation between the MTJMSD features and AFM cantilever. We noted that before interacting with SMMs, a bare MTJ showed moderate magnetic contrast in the MFM scan (Fig. 5b). However, it was extremely challenging to get any conclusive MFM image and notice a substantial change in MFM contrast due to SMMs. We also employed Ferromagnetic Resonance (FMR) to study the SMM impact on an array of ~20,000 MTJ cylindrical pillars. Sample preparation for the MTJ pillars was in accordance with our previously reported lift-off-based method ^{5a}. FMR study was performed with NanoOsc Phase FMR at 10 GHz microwave frequency. FMR showed two overlapping resonance for the MTJ (Fig. 5c). FMR signal did not change noticeably after SMM interaction with the MTJ pillars. We surmise that either SMM was unable to impact the large enough population of 20,000 MTJ to produce detectable FMR signal, or SMM coupling between the two electrodes was not strong enough to provide a stable and noticeable change in the FMR signal. MFM and FMR were done at room temperature. In the future study, we plan to do low-temperature magnetic studies to understand the SMM effects on ferromagnetic electrodes.

To understand the role of SMM in transforming MTJ, we conducted Monte Carlo simulations (MCS). Generic MCS details about our approach are published elsewhere ^{5a}. We represented the SMM-MTJMSD with a 7x10x10 Ising model, a not to scale schematic is shown in Supplementary Material Fig. S6. Each ferromagnetic electrode was attributed to 3x10x10 dimension model, containing 300 atoms. A rim of molecules of 10x10 dimension was sandwiched between two ferromagnets (Supplementary Material Fig. S6). In our prior work, we

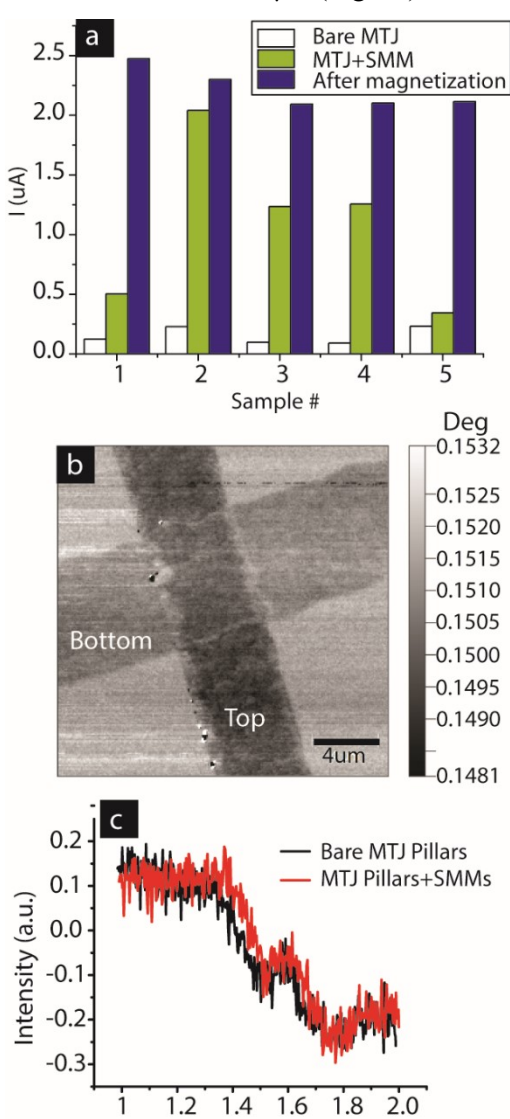


Fig. 5: (a) SMM-MTJMSD showing magnetization's effect. (b) MFM of bare MTJ (c) FMR of an array of MTJ pillars before and after treating them with SMM.

utilized such model to provide insights and explanation for the experimentally observed molecule induced strong exchange coupling effect 5a . For the present case, the interaction of molecules, placed along the central plane just along the edges, was parametrically defined by the exchange coupling parameters. For the present case, the interaction of molecules, placed along the central plane just along the edges, was parametrically defined by the exchange coupling parameters. A unit vector represented the spin of each ferromagnetic electrode atoms and molecule. The initial state of the model was that all the spin vector was aligned in the same direction. The molecule interaction with the top and the bottom ferromagnetic layer was termed as J_{SMM-T} and J_{SMM-B} , respectively. The energetics of reaching an equilibrium magnetic state of the MTJMSD can be defined by the equation 1.

$$E(MTJMSD) = -J_{Top} \left(\sum_{i \in Top} \vec{S}_i \vec{S}_{i+1} \right) - J_{Bot} \left(\sum_{i \in Bot} \vec{S}_i \vec{S}_{i+1} \right) - J_{SMM-T} \left(\sum_{i \in Top, i+1 \in SMM} \vec{S}_i \vec{S}_{i+1} \right)$$

$$-J_{SMM-B} \left(\sum_{i-1 \in SMM, i \in Bot} \vec{S}_{i-1} \vec{S}_i \right) [Eq. 1]$$

In Eq.1 atoms of ferromagnetic electrodes and molecules are represented by the spin vector S. In the expression for E(MTJMSD) the J_{Top} , and J_{Bot} , are the Heisenberg exchange coupling strengths for the top and bottom ferromagnetic electrodes, respectively. The role of J_{Top} , and J_{Bot} is very critical in MTJMSD. These two parameters are the sole reason for propagating the effect of SMM's induced exchange coupling from the tunnel junction edges to interior parts of the Ni electrodes. Each SMM molecule simultaneously connected top and bottom ferromagnetic electrodes as per the schematic is shown in Fig. 1b and the atomistic model discussed in the supplementary material (Fig. S6). We varied the sign and magnitude of these J_{SMM-T} and J_{SMM-B} parameters and measured the MTJMSD's magnetization ground state. The positive and negative sign of the exchange coupling parameters represented ferromagnetic and antiferromagnetic coupling, respectively. In the initial state, all the spin vectors were aligned in the same direction 5a . When J_{SMM-T} and J_{SMM-B} were 0, two ferromagnets were uncoupled. As thermal energy (kT) increased

magnetization kept decreasing and around kT = 1, Curie temperature, MTJMSD magnetization became zero (Fig. 6a). For the cases when both J_{SMM-T} and J_{SMM-B} were positive MTJMSD magnetization increased at a given kT with increasing coupling strengths, as compared to the case when $J_{SMM-B} = J_{SMM-T} = 0$ (Fig. 6a). We studied $J_{SMM-T} = J_{SMM-B} = 0.1$, 0.25, 0.5, 0.75, and 1 to observe any potential transition. Increasing coupling strengths decreased spin fluctuations. However, increasing magnetization cannot explain the current suppression. According to well-established spin valve theory ^{16a, 18} and Petrov¹⁹ work, magnetic leads have to be antiparallel to each other to produce the least current state on an MTJ.

We calculated the magnetization for the case when J_{SMM-T} was of the opposite sign with respect to J_{SMM-B} (Fig. 6b). The magnitude of both parameters was equal and was the same as used for Fig. 6b. When the magnitude of J_{SMM-T} and J_{SMM-B} was less than 0.25, the MTJMSD's magnetization showed negligible change with respect to the case when two magnetic layers were uncoupled J_{SMM-T} = $J_{SMM-B} = 0$. However, for the weak coupling, the MTJMSD's magnetization was significantly noisy, indicating that two ferromagnets were switching among various magnetic alignments at fixed kT. As molecular coupling strength was 0.25 overall MTJMSD's magnetization started settling in the magnetization because two nearzero

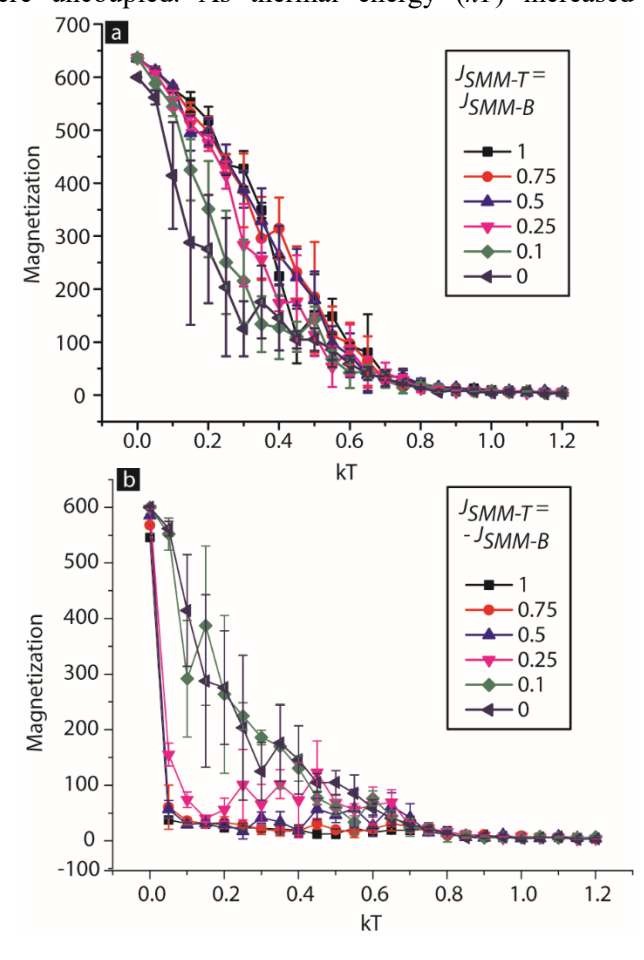


Fig. 6: Magnetization versus thermal energy (kT) graph for 3D Ising model of SMM based MTJMSD when J_{SMM-T} and J_{SMM-B} are of same magnitude with (a) same sign and (b) opposite sign.

ferromagnetic electrodes are preferably aligned in opposite directions. However, 0.25 is still not strong enough to make two ferromagnet aligned perfectly antiparallel at different kT. In this state, two electrodes cancel the magnetization of each other ¹⁸. This molecule induced antiparallel state which is also responsible for the suppressed current state ^{5b, 7a}. However, if molecular coupling strength is in between 0.1 and 0.25 overall MTJMSD may be in an unstable state (Fig. 6b). At a given thermal energy, an MTJMSD may switch back and forth in the low and high current state, like the phenomenon observed in this paper. If the magnitude of molecular coupling strength increases beyond 0.25 very stable antiparallel alignment of ferromagnetic layers will be achieved and will be observed from the decreased magnetization ^{5a}. In such cases, an MTJMSD will exhibit current suppression ^{5b, 7a}. In the previous study with a different type of paramagnetic molecule produced strong antiferromagnetic exchange coupling between two ferromagnetic electrodes leading to room temperature current suppression and long-range impact on magnetic properties of the ferromagnetic electrodes ^{5a, 7a}.

One may argue that Ni ferromagnets used in this study are not 100% spin polarized. In the generic MCS discussed here, we represented did not account for this conventional fact about Ni. However, a large number of studies have demonstrated that the degree of spin polarization of a ferromagnetic electrode is a strong function of the inter-ferromagnetic electrode coupling^{9, 20}. In the present case, we surmise that SMM serves the role of a spin filtering agent impacting the spin polarization of the Ni. An SMM also strongly couple the Ni electrodes to yield strong exchange coupling governing the alignment of the spin-polarized Ni electrodes. However, at the higher thermal energy, the molecular coupling may make Ni electrode alignment switching between parallel and antiparallel state, like the one seen in Fig. 6b. Present SMM-MTJMSD appears to be more stable in the higher current state as compared to the suppressed current state.

Conclusion: We demonstrated the use of MTJ testbed-based approach for studying molecular systems with SMM behavior. I-V studies were performed at room temperature and showed that SMM generally increased the current of host MTJs. Several MTJs also showed a temporary current suppression phenomenon. Magnetizing the SMM based MTJMSD stabilized the high current state. This study showed that device yield could approach 100% and mainly depended on the quality and availability of the MTJs/chip. We also formed MTJMSD in a way that does not lead to oxidation of nickel ferromagnet. It is noteworthy that oxidation of the ferromagnet is cited as a major obstacle in fabricating molecular devices. SMM based MTJMSD's produced a transient current suppression by several orders of magnitude. Future studies will provide several new insights when MTJ employs various types of ferromagnetic electrodes and other varieties of the SMMs. In the future, we plan to pursue low-temperature transport study under varying magnetic field and light radiation to explore SMMs' quantum state impact on transport and realizing magneto resistance like switching mechanisms. Besides, we plan to conduct magnetometry on MTJMSDs with different ferromagnetic electrode compositions to create the difference in magnetic anisotropy and saturation field. Such variation in ferromagnetic electrodes is expected to enable SMMs to yield different impact on MTJMSDs.

Acknowledgement: The preparation of this paper was in part supported by National Science Foundation-CREST Award (Contract # HRD- 1914751), Department of Energy/ National Nuclear Security Agency (DE-FOA-0003945), and Air Force Office of Sponsored Research (Award #FA9550-13-1-0152). We also thank National Institute of Standards and Technology (NIST) at Gaithersburg, Maryland in the USA for providing access to the nanotechnology resources at Center of Nanoscale Science and Technology (CNST). Financial support from the Spanish Ministry of Science, Innovation and Universities [projects CTQ2016-75068P and MDM-2015-0538 (Excellence Unit "María de Maeztu")] is also gratefully acknowledged. J.M.L. thanks the "Ramón y Cajal" Programme. Any opinions, findings, and conclusions expressed in this material are those of the author (s) and do not necessarily reflect the views of any funding agency and corresponding author's past and present affiliations.

References:

- 1. (a) Leuenberger, M. N.; Mucciolo, E. R., Berry-phase oscillations of the kondo effect in single-molecule magnets. *Phys. Rev. Lett.* **2006**, *97* (12), 126601; (b) Bogani, L.; Wernsdorfer, W., Molecular spintronics using single-molecule magnets. *Nat. Mater.* **2008**, *7* (3), 179-186.
- 2. (a) Affronte, M.; Troiani, F.; Ghirri, A.; Candini, A.; Evangelisti, M.; Corradini, V.; Carretta, S.; Santini, P.; Amoretti, G.; Tuna, F.; Timco, G.; Winpenny, R. E. P., Single molecule magnets for quantum computation. *J. Phys. D-Appl. Phys.* **2007**, *40* (10), 2999-3004; (b) Coronado, E.; Epsetin, A. J., Molecular spintronics and quantum computing. *J. Mater. Chem.* **2009**, *19* (12), 1670-1671; (c) Bartolome, J.; Luis, F.; Fernandez, J. F., *Molecular Magnets: Physics and Applications*. Springer: 2014.
- 3. Heersche, H. B.; de Groot, Z.; Folk, J. A.; van der Zant, H. S. J.; Romeike, C.; Wegewijs, M. R.; Zobbi, L.; Barreca, D.; Tondello, E.; Cornia, A., Electron transport through single Mn-12 molecular magnets. *Phys. Rev. Lett.* **2006**, *96* (20), 206801.
- 4. (a) Cinchetti, M.; Dediu, V. A.; Hueso, L. E., Activating the molecular spinterface. *Nat Mater* **2017**, *16* (5), 507-515; (b) Sanvito, S., MOLECULAR SPINTRONICS The rise of spinterface science. *Nat. Phys.* **2010**, *6* (8), 562-564.
- 5. (a) Tyagi, P.; Baker, C.; D'Angelo, C., Paramagnetic Molecule Induced Strong Antiferromagnetic Exchange Coupling on a Magnetic Tunnel Junction Based Molecular Spintronics Device. *Nanotechnology* **2015**, *26*, 305602; (b) Tyagi, P.; Friebe, E., Large Resistance Change on Magnetic Tunnel Junction based Molecular Spintronics Devices. *J. Mag. Mag. Mat.* **2018**, *453*, 186-192.
- 6. Tyagi, P.; Friebe, E.; Baker, C., Addressing The Challenges Of Using Ferromagnetic Electrodes In The Magnetic Tunnel Junction-Based Molecular Spintronics Devices. *J.Nanoparticle Res.* **2015**, *17* (11), 452.
- 7. (a) Tyagi, P.; Riso, C.; Friebe, E., Magnetic Tunnel Junction Based Molecular Spintronics Devices Exhibiting Current Suppression At Room Temperature. *Organic Electronics* **2019**, *64*, 188-194; (b) Tyagi, P.; Riso, C., Molecular spintronics devices exhibiting properties of a solar cell. *Nanotechnology* **2019**, *30* (49), 495401; (c) Tyagi, P.; Riso, C., Magnetic force microscopy revealing long range molecule impact on magnetic tunnel junction based molecular spintronics devices. *Organic Electronics* **2019**, *75*, 105421.
- 8. Tyagi, P.; Li, D. F.; Holmes, S. M.; Hinds, B. J., Molecular Electrodes At The Exposed Edge Of Metal/Insulator/Metal Trilayer Structures. *J. Am. Chem. Soc.* **2007**, *129* (16), 4929-4938.
- 9. Pasupathy, A. N.; Bialczak, R. C.; Martinek, J.; Grose, J. E.; Donev, L. A. K.; McEuen, P. L.; Ralph, D. C., The Kondo effect in the presence of ferromagnetism. *Science* **2004**, *306* (5693), 86-89.
- 10. Rojas-Dotti, C.; Martínez-Lillo, J., Thioester-functionalised and oxime-based hexametallic manganese(III) single-molecule magnets. *RSC Advances* **2017**, *7* (77), 48841-48847.
- 11. (a) Tomsa, A.-R.; Martínez-Lillo, J.; Li, Y.; Chamoreau, L.-M.; Boubekeur, K.; Farias, F.; Novak, M. A.; Cremades, E.; Ruiz, E.; Proust, A., A new family of oxime-based hexanuclear manganese (III) single molecule magnets with high anisotropy energy barriers. *Chem. Comm.* **2010**, *46* (28), 5106-5108; (b) Martínez-Lillo, J.; Dolan, N.; Brechin, E. K., A family of cationic oxime-based hexametallic manganese (III) single-molecule magnets. *Dalton Transactions* **2014**, *43* (11), 4408-4414; (c) Martínez-Lillo, J.; Cano, J.; Wernsdorfer, W.; Brechin, E. K., The Effect of Crystal Packing and ReIV Ions on the Magnetisation Relaxation of [Mn6]-Based Molecular Magnets. *Chemistry—A European Journal* **2015**, *21* (24), 8790-8798.
- 12. (a) Tyagi, P.; Li, D.; Holmes, S. M.; Hinds, B. J. In *Insulator Film Thickness to Fix the Spacing between Electrodes to Molecular Length Scale*, Nano/Micro Engineered and Molecular Systems, 2007. NEMS'07. 2nd IEEE International Conference on, IEEE: 2007; pp 191-194; (b) Tyagi, P.; Hinds, B. J., Mechanism of Ultrathin Tunnel Barrier Failure Due to Mechanical Stress Induced Nano-Sized Hillocks and Voids. *J. Vac. Sci. Technol. B* **2010**, *28* (5), 517-521; (c) Tyagi, P.; Friebe, E.; Jacquis, B.; Goulet, T.; Travers, S.; Garcia

Moreno, F., Taguchi Design of Experiment Enabling the Reduction of Spikes on the Sides of Patterned Thin Films for Tunnel Junction Fabrication. *MRS Advances* **2017**, *2* (52), 3025-3030

- 13. (a) Åkerman, J. J.; Escudero, R.; Leighton, C.; Kim, S.; Rabson, D.; Dave, R. W.; Slaughter, J.; Schuller, I. K., Criteria for ferromagnetic–insulator–ferromagnetic tunneling. *J.Mag. Mag. Mat.* **2002**, *240* (1-3), 86-91; (b) Miller, C. W.; Li, Z.-P.; Åkerman, J.; Schuller, I. K., Impact of interfacial roughness on tunneling conductance and extracted barrier parameters. *Applied physics letters* **2007**, *90* (4), 043513.
- 14. Tyagi, P., Multilayer Edge Molecular Electronics Devices: A Review. *J. Mater. Chem.* **2011,** *21* (13), 4733-4742.
- 15. (a) Hu, B. *PhD Thesis: Fabrication and Study of Molecular Devices and Photovoltaic Devices by Metal/Dielectrc/Metal Structures*; University of Kentucky (http://uknowledge.uky.edu/cgi/viewcontent.cgi?article=1224&context=gradschool_diss): University of Kentucky, 2011; (b) Ashwell, G. J.; Wierzchowiec, P.; Bartlett, C. J.; Buckle, P. D., Molecular electronics: connection across nano-sized electrode gaps. *Chem. Commun.* 2007, (12), 1254-1256.
- 16. (a) Miao, G. X.; Munzenberg, M.; Moodera, J. S., Tunneling path toward spintronics. *Rep. Prog. Phys.* **2011**, *74*, 036501; (b) Yuasa, S.; Djayaprawira, D., Giant tunnel magnetoresistance in magnetic tunnel junctions with a crystalline MgO (0 0 1) barrier. *J. Phys. D: App. Phys.* **2007**, *40* (21), R337.
- 17. Moodera, J. S.; Nassar, J.; Mathon, G., Spin-tunneling in ferromagnetic junctions. *Ann. Rev. Mater. Sci.* **1999**, *29*, 381-432.
- 18. Yuasa, S., Giant tunneling magnetoresistance in MgO-based magnetic tunnel junctions. *J.Phys. Soc. Jpn.* **2008**, *77* (3), 031001.
- 19. Petrov, E. G.; Tolokh, I. S.; May, V., Magnetic field control of an electron tunnel current through a molecular wire. *J. Chem. Phys.* **1998**, *108* (11), 4386-4396.
- 20. (a) Martinek, J.; Sindel, M.; Borda, L.; Barnas, J.; Konig, J.; Schon, G.; von Delft, J., Kondo effect in the presence of itinerant-electron ferromagnetism studied with the numerical renormalization group method. *Phys. Rev. Lett.* **2003**, *91* (24), 247202; (b) Tiusan, C.; Faure-Vincent, J.; Sicot, M.; Hehn, M.; Bellouard, C.; Montaigne, R.; Andrieu, S.; Schuhl, A., Spin filtering effects in monocristalline Fe/MgO/Fe magnetic tunnel junctions. *Materials Science and Engineering B-Solid State Materials for Advanced Technology* **2006**, *126* (2-3), 112-119.